Finite element simulation of eddy current problems using magnetic scalar potentials

Ana Alonso Rodríguez[1a], Enrico Bertolazzi[b], Riccardo Ghiloni[a], Alberto Valli[a]

[a] *Dipartimento di Matematica, Università di Trento, Italy.*
[b] *Dipartimento di Ingegneria Meccanica e Strutturale, Università di Trento, Italy.*

Abstract

We propose a new implementation of the finite element approximation of eddy current problems using as principal unknown the magnetic field. In the non-conducting region a scalar magnetic potential is introduced. The method can deal automatically with any topological configuration of the conducting region and, being based on the search of a scalar magnetic potential in the non-conducting region, has the advantage of making use of a reduced number of unknowns. Several numerical tests are presented for illustrating the performance of the proposed method; in particular, the numerical simulation of a new type of transformer of complicated topological shape is shown.

Keywords: Eddy current problem, finite element, loop fields, source field, algebraic topology methods.
2010 MSC: 65N30, 78M10, 55N99

1. Introduction

Eddy current equations are a well-known approximation of Maxwell equations obtained by disregarding the displacement current term; as a consequence, wave propagation phenomena are not taken into account, and only diffusion of electromagnetic fields is considered.

This is typically the case of "slow" fields, or of low frequency time-harmonic problems, usually appearing in electrotechnics. For instance, induction heating, transformers, magnetic levitation, non-destructive testing, biomedical identification problems can be modeled by the eddy current equations.

Many papers have been devoted to the numerical simulation of these problems: let us only refer to the book by Alonso Rodríguez and Valli [1] and to the references therein.

As it is well-known, the time-dependent Maxwell equations read:

$$\begin{cases} \dfrac{\partial \mathcal{D}}{\partial t} - \operatorname{curl} \mathcal{H} = -\mathcal{J} & \text{Maxwell–Ampère equation} \\ \dfrac{\partial \mathcal{B}}{\partial t} + \operatorname{curl} \mathcal{E} = 0 & \text{Faraday equation}\,, \end{cases} \tag{1}$$

where the physical quantities that appear are the magnetic field $\mathcal{H}$, the electric field $\mathcal{E}$, the magnetic induction $\mathcal{B}$, the electric induction $\mathcal{D}$ and the electric current density $\mathcal{J}$.

When the problem is driven by an applied current density $\mathcal{J}_e$, one needs to consider the generalized Ohm law $\mathcal{J} = \boldsymbol{\sigma}\mathcal{E} + \mathcal{J}_e$, where $\boldsymbol{\sigma}$ is the electric conductivity (vanishing in non-conducting regions). Moreover, a linear dependence of the form $\mathcal{D} = \boldsymbol{\varepsilon}\mathcal{E}$, $\mathcal{B} = \boldsymbol{\mu}\mathcal{H}$ is usually assumed; here $\boldsymbol{\varepsilon}$ and $\boldsymbol{\mu}$ are the electric permittivity and magnetic permeability, respectively. In many physical and engineering problems, the region of interest is composed of a non-homogeneous and non-isotropic medium: therefore, $\boldsymbol{\sigma}$, $\boldsymbol{\varepsilon}$ and $\boldsymbol{\mu}$ are not constant, but are symmetric and uniformly positive definite matrices (with entries that are bounded functions of the space variable).

[1] Corresponding author; e-mail: alonso@science.unitn.it

The system of equations obtained when the displacement current term $\frac{\partial \mathcal{D}}{\partial t}$ is disregarded is the eddy current system:

$$\begin{cases} \operatorname{curl} \mathcal{H} = \boldsymbol{\sigma} \mathcal{E} + \mathcal{J}_e \\ \boldsymbol{\mu} \dfrac{\partial \mathcal{H}}{\partial t} + \operatorname{curl} \mathcal{E} = 0 \,. \end{cases} \tag{2}$$

Though the same approach we are going to proposed can be used for the time-dependent case, for the sake of simplicity in this paper we prefer to focus on the time-harmonic case, namely, the applied current density $\mathcal{J}_e$ is an alternating current, having the form $\mathcal{J}_e(\mathbf{x}, t) = \mathbf{J}_*(\mathbf{x}) \cos(\omega t + \phi)$, where $\mathbf{J}_*(\mathbf{x})$ is a real-valued vector function, $\omega \neq 0$ is the angular frequency and ϕ is the phase angle. This is equivalent to the representation

$$\mathcal{J}_e(\mathbf{x}, t) = \operatorname{Re}\left[\mathbf{J}_*(\mathbf{x}) e^{\imath(\omega t + \phi)}\right] = \operatorname{Re}\left[\mathbf{J}_e(\mathbf{x}) e^{\imath \omega t}\right] \,,$$

where we have introduced the complex-valued vector function $\mathbf{J}_e(\mathbf{x}) := \mathbf{J}_*(\mathbf{x}) e^{\imath \phi}$.

Accordingly, we look for a time-harmonic solution given by

$$\mathcal{E}(\mathbf{x}, t) = \operatorname{Re}\left[\mathbf{E}(\mathbf{x}) e^{\imath \omega t}\right] \quad , \quad \mathcal{H}(\mathbf{x}, t) = \operatorname{Re}\left[\mathbf{H}(\mathbf{x}) e^{\imath \omega t}\right] \,,$$

and the time-harmonic eddy current equations, derived from (2) under these assumptions, read

$$\begin{cases} \operatorname{curl} \mathbf{H} = \boldsymbol{\sigma} \mathbf{E} + \mathbf{J}_e \\ \operatorname{curl} \mathbf{E} + \imath \omega \boldsymbol{\mu} \mathbf{H} = \mathbf{0} \,. \end{cases} \tag{3}$$

Note that for the uniqueness of the electric field in the non-conducting region one needs additional conditions. However we are not interested in the computation of that quantity, hence the reader interested to the complete system can refer to Alonso Rodríguez and Valli [1].

For solving these equations, the most popular approaches are based on vector potentials. Denoting by Ω_C the conducting region and by Ω_I the non-conducting region, the most classical method is that using a vector potential $\mathbf{A}$ of the magnetic induction $\boldsymbol{\mu}\mathbf{H}$ in the whole computational domain Ω and a scalar electric potential V_C in the conducting region Ω_C, satisfying $\operatorname{curl} \mathbf{A} = \boldsymbol{\mu}\mathbf{H}$ in Ω and $-\operatorname{grad} V_C = \mathbf{E}_{|\Omega_C} + \imath\omega \mathbf{A}_{|\Omega_C}$ in Ω_C.

For numerical approximation this approach is rather expensive, as one has to discretize a vector field in the whole domain and a scalar function in the conducting region. Moreover, if classical Lagrange nodal elements are used for the approximation of each single component of $\mathbf{A}$, gauging is compulsory (namely, additional restriction on $\mathbf{A}$ have to be introduced); moreover, the efficiency of the scheme is not guaranteed in the presence of re-entrant corners (see, e.g., Costabel et al. [2]). On the other hand, if edge elements are employed for the approximation of the complete vector field $\mathbf{A}$, a Lagrange multiplier has to be introduced or the resulting linear system turns out to be singular, and in any case it needs special care for being solved.

An alternative approach, with a smaller number of unknowns, is to use the formulation in terms of the magnetic field and to introduce a scalar magnetic potential in the non-conducting region, (see, e.g., Bossavit [3], Bermúdez et al. [4], Alonso Rodríguez and Valli [1]). In general topological situations this scalar magnetic potential is in fact a multivalued function. More precisely it is known that if the insulator is not simply-connected there are closed curves contained in Ω_I that are not the boundary of any surface contained in Ω_I; the space of scalar magnetic potentials includes multivalued functions with a constant jump across suitable surfaces "cutting" the non-bounding cycles of Ω_I. The identification of such surfaces can be a difficult task; however the key point is that the gradients of these multivalued functions are loop fields, namely, curl-free vector fields whose line integral on at least one closed curve contained in Ω_I is different from 0 (this closed curve is precisely the non-bounding cycle cut by the surface).

The algorithm presented in this paper does not need the determination of these "cutting" surfaces, and it is simply based on the knowledge of a basis of loop fields. In particular, we can use the maximal set of independent loop fields provided for any bounded domain Ω_I by the general algorithm derived in Alonso Rodríguez et al. [5]. It is worth noting that this algorithm determines the loop fields using only the knowledge of the vertices and the tetrahedra of the mesh, and of the mesh induced on the boundary of Ω_I.

The paper is organized as follow. In Section 2 we decompose the magnetic field in the non-conducting as the sum of the gradient of a (genuine) function, a loop field and a source field. Then we write the variational formulation of the eddy current problem in terms of the magnetic field. Section 3 is devoted to the finite element approximation of this formulation, the derivation of the resulting algebraic system and the description of a preconditioned iterative method to solve it. Finally, Section 4 contains numerical experiments that show the performance of the proposed algorithm.

2. Formulation via a scalar magnetic potential

A peculiar aspect of eddy current equations is that, in the non-conducting region, they reduce to a constraint on the curl of the magnetic field: $\operatorname{curl} \mathbf{H}_{|\Omega_I} = \mathbf{J}_{e|\Omega_I}$. Therefore, one is led to a two-step procedure: first, determine a vector potential $\mathbf{H}_{e,I}$ of $\mathbf{J}_{e|\Omega_I}$; second, introduce a scalar magnetic potential ψ_I such that $\operatorname{grad} \psi_I = \mathbf{H}_{|\Omega_I} - \mathbf{H}_{e,I}$.

The second step is subjected to well-known topological restrictions: a curl-free vector field in Ω_I is equal to a gradient if and only if the domain Ω_I is homologically trivial or, equivalently, simply-connected (see Benedetti et al. [6] for this equivalence result). Very often, in real-life computational problems this is not the case, as the conducting region is not simply-connected (and consequently Ω_I is not simply-connected, whatever topological shape has the whole domain Ω).

For general domains Ω_C and Ω_I, a curl-free vector field is given by a gradient plus a *loop field*, namely, a curl-free vector field whose line integral on some loops (closed curves) contained in Ω_I is different from 0.

In algebraic topology, the space of loop fields in Ω_I or, better, the curl-free vector fields in Ω_I modulo gradients, is called first de Rham cohomology group Ω_I and it is known that its dimension is equal to g, the first Betti number of Ω_I. Assume that we know a basis for this space, given by g vector fields $\mathbf{T}^I_{0,n}$, $n = 1, \dots, g$. Then we can write

$$\mathbf{H}_{|\Omega_I} = \mathbf{H}_{e,I} + \operatorname{grad} \psi_I + \sum_{n=1}^{g} d_n \mathbf{T}^I_{0,n} \,,$$

and, besides the function ψ_I, one has g additional unknowns, the complex numbers d_n.

We will see that a similar situation occurs when one discretizes the eddy current problem by means of finite elements. In that case, one has to find a source field, namely, a finite element vector field $\mathbf{H}_{e,h}$ such that $\operatorname{curl} \mathbf{H}_{e,h|\Omega_I} = \mathbf{J}^I_{e,h}$, being $\mathbf{J}^I_{e,h}$ a suitable approximation of $\mathbf{J}_{e|\Omega_I}$, and a finite element basis for the first de Rham cohomology group of Ω_I.

2.1. Variational formulation

In this section we consider a set Ω that is a bounded and connected open subset of $\mathbb{R}^3$ with Lipschitz boundary $\partial\Omega$. A conducting region Ω_C, an open and not necessarily connected set with Lipschitz boundary, is strictly contained in Ω (i.e., $\overline{\Omega_C} \subset \Omega$). The non-conducting region $\Omega_I = \Omega \setminus \overline{\Omega_C}$ is assumed to be connected but not necessarily simply-connected (this means that at least one of the connected comnponents of Ω_C can be not simply-connected). We set $\Gamma = \partial\Omega_C = \partial\Omega_C \cap \partial\Omega_I$; therefore, under these assumptions we have $\partial\Omega_I = \Gamma \cup \partial\Omega$. We also recall that the electric conductivity $\boldsymbol{\sigma}$ is vanishing in Ω_I.

The classical Sobolev spaces are employed: in particular, $L^2(\Omega)$ is the space of complex-valued functions defined in Ω that are measurable and square integrable, and

$$\begin{aligned} H^1(\Omega) &= \{\phi \in L^2(\Omega) \mid \operatorname{grad} \phi \in (L^2(\Omega))^3\} \,, \\ H(\operatorname{curl};\Omega) &= \{\mathbf{v} \in (L^2(\Omega))^3 \mid \operatorname{curl} \mathbf{v} \in (L^2(\Omega))^3\} \,, \\ H(\operatorname{div};\Omega) &= \{\mathbf{v} \in (L^2(\Omega))^3 \mid \operatorname{div} \mathbf{v} \in L^2(\Omega)\} \,. \end{aligned}$$

We consider the eddy current problem with a perfect conducting boundary, namely,

$$\begin{cases} \operatorname{curl} \mathbf{H} = \boldsymbol{\sigma}\mathbf{E} + \mathbf{J}_e & \text{in } \Omega \\ \operatorname{curl} \mathbf{E} + \imath\omega\boldsymbol{\mu}\mathbf{H} = \mathbf{0} & \text{in } \Omega \\ \mathbf{E} \times \mathbf{n} = \mathbf{0} & \text{on } \partial\Omega \,, \end{cases} \tag{4}$$

$\mathbf{n}$ being the unit outward normal vector on $\partial\Omega_I = \Gamma \cup \partial\Omega$. Since the density current $\mathbf{J}_e$ must be equal to $\operatorname{curl}\mathbf{H}$ in Ω_I, for the sake of solvability it has to satisfy some additional conditions. For expressing them, let us indicate by Γ_j, $j = 1, \ldots, p_\Gamma + 1$, the connected components of Γ, and by $(\partial\Omega)_r$, $r = 0, 1, \ldots, p_{\partial\Omega}$, the connected components of $\partial\Omega$ (in particular, we have denoted by $(\partial\Omega)_0$ the external one). The density current must satisfy

$$\begin{array}{ll} \operatorname{div}\mathbf{J}_{e|\Omega_I} = 0 & \text{in } \Omega_I \\ \int_{\Gamma_j} \mathbf{J}_{e|\Omega_I} \cdot \mathbf{n} = 0 & \forall\, j = 1, \ldots, p_\Gamma \\ \int_{(\partial\Omega)_r} \mathbf{J}_{e|\Omega_I} \cdot \mathbf{n} = 0 & \forall\, r = 0, 1, \ldots, p_{\partial\Omega}\,. \end{array} \tag{5}$$

A variational formulation of (4) is easily devised. Having introduced the space

$$Z = \{\mathbf{v} \in H(\operatorname{curl};\Omega) \mid \operatorname{curl}\mathbf{v}_{|\Omega_I} = \mathbf{0} \text{ in } \Omega_I\}\,,$$

by integration by parts for each $\mathbf{v} \in Z$ one has

$$\begin{aligned} -\imath\omega \textstyle\int_\Omega \boldsymbol{\mu}\mathbf{H}\cdot\mathbf{v} &= \textstyle\int_\Omega \operatorname{curl}\mathbf{E}\cdot\mathbf{v} = \int_\Omega \mathbf{E}\cdot\operatorname{curl}\mathbf{v} + \int_{\partial\Omega} \mathbf{n}\times\mathbf{E}\cdot\mathbf{v} \\ &= \textstyle\int_{\Omega_C} \mathbf{E}\cdot\operatorname{curl}\mathbf{v} = \int_{\Omega_C} \boldsymbol{\sigma}^{-1}(\operatorname{curl}\mathbf{H} - \mathbf{J}_e)\cdot\operatorname{curl}\mathbf{v}\,. \end{aligned} \tag{6}$$

Let $\mathbf{H}_e \in H(\operatorname{curl};\Omega)$ be such that $\operatorname{curl}\mathbf{H}_{e|\Omega_I} = \mathbf{J}_{e|\Omega_I}$ (i.e., $\mathbf{H}_{e|\Omega_I}$ is a vector potential of $\mathbf{J}_{e|\Omega_I}$; conditions (5) are equivalent to the existence of such a potential). Then we can write $\mathbf{H} = \mathbf{Z} + \mathbf{H}_e$ with $\mathbf{Z} \in Z$, and therefore we can rewrite (6) as follows:

$$\begin{aligned} -\imath\omega \textstyle\int_\Omega \boldsymbol{\mu}(\mathbf{Z}+\mathbf{H}_e)\cdot\mathbf{v} &= \textstyle\int_{\Omega_C} \boldsymbol{\sigma}^{-1}[\operatorname{curl}(\mathbf{Z}+\mathbf{H}_e) - \mathbf{J}_e)]\cdot\operatorname{curl}\mathbf{v} \\ &= \textstyle\int_{\Omega_C} \boldsymbol{\sigma}^{-1}\operatorname{curl}\mathbf{Z}\cdot\operatorname{curl}\mathbf{v} + \int_{\Omega_C} \boldsymbol{\sigma}^{-1}(\operatorname{curl}\mathbf{H}_e - \mathbf{J}_e)\cdot\operatorname{curl}\mathbf{v}\,. \end{aligned}$$

In conclusion, we have obtained the variational problem

$$\begin{array}{l} \text{Find } \mathbf{Z} \in Z \ : \\ \quad \int_{\Omega_C} \boldsymbol{\sigma}^{-1}\operatorname{curl}\mathbf{Z}\cdot\operatorname{curl}\mathbf{v} + \imath\omega\int_\Omega \boldsymbol{\mu}\mathbf{Z}\cdot\mathbf{v} \\ \qquad\qquad = -\int_{\Omega_C} \boldsymbol{\sigma}^{-1}(\operatorname{curl}\mathbf{H}_e - \mathbf{J}_e)\cdot\operatorname{curl}\mathbf{v} - \imath\omega\int_\Omega \boldsymbol{\mu}\mathbf{H}_e\cdot\mathbf{v} \\ \text{for all } \mathbf{v} \in Z\,. \end{array} \tag{7}$$

It is easy to see that problem (7) has a unique solution (see, e.g., Alonso Rodríguez and Valli [1], Sect. 3.1).

3. Finite element approximation

In this section the domains Ω, Ω_C and Ω_I are polyhedral domains. We introduce a tetrahedral triangulation $\mathcal{T}_h = (V, E, F, T)$ of $\overline{\Omega}$; here V is the set of vertices, E the set of edges, F the set of faces and T the set of tetrahedra in $\mathcal{T}_h$.

We assume that $\mathcal{T}_h$ induces a triangulation $\mathcal{T}_h^C = (V^C, E^C, F^C, T^C)$ of $\overline{\Omega_C}$, a triangulation $\mathcal{T}_h^I = (V^I, E^I, F^I, T^I)$ of $\overline{\Omega_I}$, and a triangulation $\mathcal{T}_h^\Gamma = (V^\Gamma, E^\Gamma, F^\Gamma)$ of Γ. Clearly $V^\Gamma = V^I \cap V^C$, $E^\Gamma = E^I \cap E^C$ and $F^\Gamma = F^I \cap F^C$.

If $v_1, \ldots, v_{n_v}$ are the elements of V, we assume that for $i = 1, \ldots, n_C$ we have $v_i \in \Omega_C$, for $i = n_C + 1, \ldots, n_C + n_I$ we have $v_i \in \Omega_I \cup \partial\Omega$ and for $i = n_C + n_I + 1, \ldots, n_C + n_I + n_\Gamma = n_v$ we have $v_i \in \Gamma$. Similarly, if $e_1, \ldots, e_{n_e}$ are the elements of E, we assume that for $j = 1, \ldots, m_C$ we have $e_j \in E^C \setminus E^\Gamma$, for $j = m_C + 1, \ldots, m_C + m_I$ we have $e_j \in E^I \setminus E^\Gamma$, and for $j = m_C + m_I + 1, \ldots, m_C + m_I + m_\Gamma = n_e$ we have $e_j \in E^\Gamma$.

We consider the following spaces of finite elements:

- The space L_h of continuous piecewise-linear Lagrange finite elements. Its dimension is n_v, the number of vertices in $\mathcal{T}_h$.

- The space N_h of Nédélec edge finite elements of degree 1. Its dimension is n_e, the number of edges in $\mathcal{T}_h$.

- The space RT_h of Raviart–Thomas finite elements of degree 1. Its dimension is n_f, the number of faces in $\mathcal{T}_h$.

It is well-known that $L_h \subset H^1(\Omega)$, $N_h \subset H(\mathrm{curl};\Omega)$ and $RT_h \subset H(\mathrm{div};\Omega)$. Moreover $\mathrm{grad}\, L_h \subset N_h$ and $\mathrm{curl}\, N_h \subset RT_h$ (see, e.g., Monk [7]).

We also denote by Π^{RT_h} and Π^{N_h} the interpolation operators valued in RT_h and N_h, respectively. These operators are defined for smooth enough functions. In particular, in the sequel we consider the Raviart–Thomas interpolant of $\mathbf{J}_{e|\Omega_I}$, and we set $\mathbf{J}^I_{e,h} = \Pi^{RT_h}\mathbf{J}_{e|\Omega_I}$.

We replace $\mathbf{H}_e$ with $\mathbf{H}_{e,h} \in N_h$ defined in the following way: having constructed as in Alonso Rodríguez et al. [5] the finite element source field $\mathbf{H}^I_{e,h}$ satisfying $\mathrm{curl}\,\mathbf{H}^I_{e,h} = \mathbf{J}^I_{e,h}$ in Ω_I, define a Nédélec finite element $\mathbf{H}_{e,h}$ by setting

$$\int_{e_j} \mathbf{H}_{e,h}\cdot\boldsymbol{\tau} = \begin{cases} 0 & \text{if } j = 1,\dots,m_C \\ \displaystyle\int_{e_j} \mathbf{H}^I_{e,h}\cdot\boldsymbol{\tau} & \text{if } j = m_C+1,\dots,n_e\,. \end{cases}$$

Notice that $\mathrm{supp}\,\mathbf{H}_{e,h} \not\subset \overline{\Omega_I}$ and that $\mathrm{curl}\,\mathbf{H}_{e,h} = \mathbf{J}^I_{e,h}$ in Ω_I but $\mathrm{curl}\,\mathbf{H}_{e,h} \neq \mathbf{J}_e$ in Ω_C.

A natural finite element approximation of the space Z is given by

$$Z_h = \{\mathbf{v}_h \in N_h \mid \mathrm{curl}\,\mathbf{v}_{h|\Omega_I} = \mathbf{0} \text{ in } \Omega_I\}\,.$$

It is important now to make clear how a basis of this space can be constructed. We denote by $\mathbf{w}_{h,j}$, $j = 1,\dots,m_C$, the Nédélec basis function for each edge e_j strictly inside Ω_C (and not on its boundary), and by $\Phi_{h,i}$, $i = n_C+1,\dots,n_v$, the Lagrange nodal basis function for each node v_i inside Ω_I or on its boundary $\partial\Omega_I = \Gamma \cup \partial\Omega$. We also consider the Nédélec finite element basis $\mathbf{T}^I_{0,n}$ of the first de Rham cohomology group of Ω_I constructed in Alonso Rodríguez et al. [5], and denote by $\mathbf{T}_{0,n}$ the extension of $\mathbf{T}^I_{0,n}$ by setting value 0 at all the degrees of freedom associated to the edges strictly inside Ω_C.

Notice that $\mathrm{supp}\,\mathbf{w}_{h,j} \subset \overline{\Omega_C}$ for $j = 1,\dots,m_C$, while $\mathrm{supp}\,\Phi_{h,i} \subset \overline{\Omega_I}$ if and only if $i = n_C+1,\dots,n_C+n_I$. Moreover, in general we cannot infer that $\mathrm{supp}\,\mathbf{T}_{0,n} \subset \overline{\Omega_I}$ and that $\mathrm{curl}\,\mathbf{T}_{0,n} = \mathbf{0}$ in Ω_C.

We easily find that

Theorem 1. *A basis of Z_h is given by*

$$\{\mathbf{w}_{h,j}\}_{j=1}^{m_C} \cup \{\mathrm{grad}\,\Phi_{h,i}\}_{i=n_C+1}^{n_v-1} \cup \{\mathbf{T}_{0,n}\}_{n=1}^{g}\,.$$

Proof. Let us start proving that any function in Z_h can be written as a linear combination of these functions. If $\mathbf{v}_h \in Z_h$, then by Theorem 3 in Alonso Rodríguez et al. [5] we have in Ω_I

$$\mathbf{v}_{h|\Omega_I} = \sum_{i=n_C+1}^{n_v-1} b_i\,\mathrm{grad}\,\Phi_{h,i|\Omega_I} + \sum_{n=1}^{g} c_n\mathbf{T}_{0,n|\Omega_I}\,.$$

On the other hand, we know that $\mathbf{v}_h$, $\mathrm{grad}\,\Phi_{h,i}$ and $\mathbf{T}_{0,n}$ are defined in the whole domain Ω and belong to N_h, hence their tangential component is continuous across Γ and we can conclude that

$$\mathbf{v}_{h|\Omega_C} - \sum_{i=n_C+1}^{n_v-1} b_i\,\mathrm{grad}\,\Phi_{h,i|\Omega_C} - \sum_{n=1}^{g} c_n\mathbf{T}_{0,n|\Omega_C}$$

is a Nédélec finite element in Ω_C with vanishing tangential component on Γ. Therefore, we can write

$$\mathbf{v}_{h|\Omega_C} - \sum_{i=n_C+1}^{n_v-1} b_i\,\mathrm{grad}\,\Phi_{h,i|\Omega_C} - \sum_{n=1}^{g} c_n\mathbf{T}_{0,n|\Omega_C} = \sum_{j=1}^{m_C} a_j\mathbf{w}_{h,j|\Omega_C}\,.$$

Since the support of $\mathbf{w}_{h,j}$ is contained in $\overline{\Omega_C}$, this relation holds also in Ω_I.

Concerning linear independence, if

$$\sum_{j=1}^{m_C} a_j \mathbf{w}_{h,j} + \sum_{i=n_C+1}^{n_v-1} b_i \operatorname{grad} \Phi_{h,i} + \sum_{n=1}^{g} c_n \mathbf{T}_{0,n} = \mathbf{0} \quad \text{in } \Omega\,,$$

in particular this same relation holds in Ω_I, hence

$$\sum_{i=n_C+1}^{n_v-1} b_i \operatorname{grad} \Phi_{h,i|\Omega_I} + \sum_{n=1}^{g} c_n \mathbf{T}_{0,n|\Omega_I} = \mathbf{0} \quad \text{in } \Omega_I\,.$$

From Theorem 3 in Alonso Rodríguez et al. [5] we find $b_i = 0$ and $c_n = 0$. We have thus obtained $\sum_{j=1}^{m_C} a_j \mathbf{w}_{h,j|\Omega_C} = \mathbf{0}$, and consequently $a_j = 0$. □

Having clarified this setting, the finite element approximation of problem (7) is readily devised. It reads

$$\begin{aligned} &\text{Find } \mathbf{Z}_h \in Z_h \ : \\ &\int_{\Omega_C} \boldsymbol{\sigma}^{-1} \operatorname{curl} \mathbf{Z}_h \cdot \operatorname{curl} \mathbf{v}_h + \imath\omega \int_\Omega \boldsymbol{\mu} \mathbf{Z}_h \cdot \mathbf{v}_h \\ &\qquad = -\int_{\Omega_C} \boldsymbol{\sigma}^{-1} (\operatorname{curl} \mathbf{H}_{e,h} - \mathbf{J}_e) \cdot \operatorname{curl} \mathbf{v}_h - \imath\omega \int_\Omega \boldsymbol{\mu} \mathbf{H}_{e,h} \cdot \mathbf{v}_h \\ &\text{for all } \mathbf{v}_h \in Z_h\,. \end{aligned} \tag{8}$$

The discrete magnetic field is given by $\mathbf{H}_h = \mathbf{Z}_h + \mathbf{H}_{e,h}$.

We easily find an optimal error estimate.

Theorem 2. *Let $\mathbf{H} = \mathbf{Z} + \mathbf{H}_e$ and $\mathbf{H}_h = \mathbf{Z}_h + \mathbf{H}_{e,h}$ be defined through the solution $\mathbf{Z}$ and $\mathbf{Z}_h$ to problems (7) and (8), respectively. Assume that $\mathbf{H}$ and $\mathbf{J}_{e|\Omega_I}$ are smooth enough, so that the interpolants $\Pi^{N_h}\mathbf{H}$ and $\Pi^{RT_h}\mathbf{J}_{e|\Omega_I}$ are defined. Then the following error estimate holds:*

$$\begin{aligned} \|\mathbf{H} - \mathbf{H}_h\|^2_{H(\operatorname{curl};\Omega)} \le C\,(&\|\mathbf{H} - \Pi^{N_h}\mathbf{H}\|^2_{H(\operatorname{curl};\Omega_C)} + \|\mathbf{H} - \Pi^{N_h}\mathbf{H}\|^2_{L^2(\Omega_I)} \\ &+ \|\mathbf{J}_e - \Pi^{RT_h}\mathbf{J}_e\|^2_{L^2(\Omega_I)})\,. \end{aligned} \tag{9}$$

Proof. Let us introduce the sesquilinear form on $Z \times Z$

$$a(\mathbf{u}, \mathbf{v}) := \int_{\Omega_C} \boldsymbol{\sigma}^{-1} \operatorname{curl} \mathbf{u} \cdot \operatorname{curl} \overline{\mathbf{v}} + \int_\Omega \imath\omega \boldsymbol{\mu} \mathbf{u} \cdot \overline{\mathbf{v}}$$

and the affine space

$$Z_h^\star = \{\mathbf{v}_h \in N_h \mid \operatorname{curl} \mathbf{v}_{h|\Omega_I} = \mathbf{J}^I_{e,h} \text{ in } \Omega_I\}\,.$$

By subtracting (8) from (7) we note that $a(\mathbf{H} - \mathbf{H}_h, \mathbf{v}_h) = 0$ for all $\mathbf{v}_h \in Z_h$, hence

$$\begin{aligned} &\|\mathbf{H} - \mathbf{H}_h\|^2_{H(\operatorname{curl};\Omega_C)} + \|\mathbf{H} - \mathbf{H}_h\|^2_{L^2(\Omega_I)} \\ &\quad \le C_1\, a(\mathbf{H} - \mathbf{H}_h, \mathbf{H} - \mathbf{H}_h) \\ &\quad = C_1\, a(\mathbf{H} - \mathbf{H}_h, \mathbf{H} - \mathbf{z}_h)\,, \end{aligned} \tag{10}$$

for each $\mathbf{z}_h \in Z_h^\star$.

Thus we have the optimal error estimate

$$\begin{aligned} &\|\mathbf{H} - \mathbf{H}_h\|^2_{H(\operatorname{curl};\Omega_C)} + \|\mathbf{H} - \mathbf{H}_h\|^2_{L^2(\Omega_I)} \\ &\quad \le C \inf_{\mathbf{z}_h \in Z_h^\star} (\|\mathbf{H} - \mathbf{z}_h\|^2_{H(\operatorname{curl};\Omega_C)} + \|\mathbf{H} - \mathbf{z}_h\|^2_{L^2(\Omega_I)})\,. \end{aligned} \tag{11}$$

Since in Ω_I the approximation of the current density is its Raviart–Thomas interpolant, namely, $\mathbf{J}^I_{e,h} = \Pi^{RT_h}\mathbf{J}_{e|\Omega_I}$, it clearly follows $\Pi^{N_h}\mathbf{H} \in Z_h^\star$, as $\operatorname{curl}(\Pi^{N_h}\mathbf{H}_{|\Omega_I}) = \Pi^{RT_h}(\operatorname{curl}\mathbf{H}_{|\Omega_I})$.

Therefore we end with (9), as $\operatorname{curl} \mathbf{H}_{|\Omega_I} = \mathbf{J}_{e|\Omega_I}$ and $\operatorname{curl} \mathbf{H}_{h|\Omega_I} = \mathbf{J}^I_{e,h} = \Pi^{RT_h} \mathbf{J}_{e|\Omega_I}$. □

As a consequence, we derive a more explicit error estimate: if $\mathbf{J}_{e|\Omega_I}$ and $\mathbf{H}$ are smooth enough, well-known interpolation results (see, e.g., Monk [7]) give that

$$\|\mathbf{H} - \mathbf{H}_h\|_{H(\operatorname{curl};\Omega)} = O(h)\,.$$

3.1. Algebraic realization

For the sake of simplicity, we multiply equation (8) by $(\imath\omega)^{-1}$. Let us define the following matrices:

$$\begin{aligned}
&A^{C,C} \in \mathbb{R}^{m_C \times m_C} \text{ for } 1 \le k, j \le m_C \\
&a^{C,C}_{k,j} = \textstyle\int_{\Omega_C} \boldsymbol{\mu} \mathbf{w}_{h,j} \cdot \mathbf{w}_{h,k}\,, \\
&B^{C,C} \in \mathbb{R}^{m_C \times m_C} \text{ for } 1 \le k, j \le m_C \\
&b^{C,C}_{k,j} = \textstyle\int_{\Omega_C} \boldsymbol{\sigma}^{-1} \operatorname{curl} \mathbf{w}_{h,j} \cdot \operatorname{curl} \mathbf{w}_{h,k}\,, \\
&A^{C,\Gamma} \in \mathbb{R}^{m_C \times (n_\Gamma - 1)} \text{ for } 1 \le k \le m_C, 1 \le r \le n_\Gamma - 1 \\
&a^{C,\Gamma}_{k,r} = \textstyle\int_{\Omega_C} \boldsymbol{\mu} \operatorname{grad} \Phi_{h,n_C+n_I+r} \cdot \mathbf{w}_{h,k}\,, \\
&A^{C,L} \in \mathbb{R}^{m_C \times g} \text{ for } 1 \le k \le m_C, 1 \le n \le g \\
&a^{C,L}_{k,n} = \textstyle\int_{\Omega_C} \boldsymbol{\mu} \mathbf{T}_{0,n} \cdot \mathbf{w}_{h,k}\,, \\
&B^{C,L} \in \mathbb{R}^{m_C \times g} \text{ for } 1 \le k \le m_C, 1 \le n \le g \\
&b^{C,L}_{k,n} = \textstyle\int_{\Omega_C} \boldsymbol{\sigma}^{-1} \operatorname{curl} \mathbf{T}_{0,n} \cdot \operatorname{curl} \mathbf{w}_{h,k}\,, \\
&A^{I,I} \in \mathbb{R}^{n_I \times n_I} \text{ for } 1 \le l, i \le n_I \\
&a^{I,I}_{l,i} = \textstyle\int_{\Omega_I} \boldsymbol{\mu} \operatorname{grad} \Phi_{h,n_C+i} \cdot \operatorname{grad} \Phi_{h,n_C+l} \\
&A^{I,\Gamma} \in \mathbb{R}^{n_I \times (n_\Gamma - 1)} \text{ for } 1 \le l \le n_I, 1 \le r \le n_\Gamma - 1 \\
&a^{I,\Gamma}_{l,r} = \textstyle\int_{\Omega_I} \boldsymbol{\mu} \operatorname{grad} \Phi_{h,n_C+n_I+r} \cdot \operatorname{grad} \Phi_{h,n_C+l} \\
&A^{I,L} \in \mathbb{R}^{n_I \times g} \text{ for } 1 \le l \le n_I, 1 \le n \le g \\
&a^{I,L}_{l,n} = \textstyle\int_{\Omega_I} \boldsymbol{\mu} \mathbf{T}_{0,n} \cdot \operatorname{grad} \Phi_{h,n_C+l} \\
&A^{\Gamma,\Gamma} \in \mathbb{R}^{(n_\Gamma - 1) \times (n_\Gamma - 1)} \text{ for } 1 \le s, r \le n_\Gamma - 1 \\
&a^{\Gamma,\Gamma}_{s,r} = \textstyle\int_{\Omega} \boldsymbol{\mu} \operatorname{grad} \Phi_{h,n_C+n_I+r} \cdot \operatorname{grad} \Phi_{h,n_C+n_I+s} \\
&A^{\Gamma,L} \in \mathbb{R}^{(n_\Gamma - 1) \times g} \text{ for } 1 \le s \le n_\Gamma - 1, 1 \le n \le g \\
&a^{\Gamma,L}_{s,n} = \textstyle\int_{\Omega} \boldsymbol{\mu} \mathbf{T}_{0,n} \cdot \operatorname{grad} \Phi_{h,n_C+n_I+s} \\
&A^{L,L} \in \mathbb{R}^{g \times g} \text{ for } 1 \le m, n \le g \\
&a^{L,L}_{m,n} = \textstyle\int_{\Omega} \boldsymbol{\mu} \mathbf{T}_{0,n} \cdot \mathbf{T}_{0,m} \\
&B^{L,L} \in \mathbb{R}^{g \times g} \text{ for } 1 \le m, n \le g \\
&b^{L,L}_{m,n} = \textstyle\int_{\Omega_C} (\omega\boldsymbol{\sigma})^{-1} \operatorname{curl} \mathbf{T}_{0,n} \cdot \operatorname{curl} \mathbf{T}_{0,m}
\end{aligned}$$

The matrix of the algebraic system expressing problem (8) is:

$$\begin{bmatrix}
A^{C,C} - \imath\omega^{-1} B^{C,C} & 0 & A^{C,\Gamma} & A^{C,L} - \imath\omega^{-1} B^{C,L} \\
0 & A^{I,I} & A^{I,\Gamma} & A^{I,L} \\
\left[A^{C,\Gamma}\right]^T & \left[A^{I,\Gamma}\right]^T & A^{\Gamma,\Gamma} & A^{\Gamma,L} \\
\left[A^{C,L}\right]^T - \imath\omega^{-1} \left[B^{C,L}\right]^T & \left[A^{I,L}\right]^T & \left[A^{\Gamma,L}\right]^T & A^{L,L} - \imath\omega^{-1} B^{L,L}
\end{bmatrix}.$$

Note that the blocks $A^{C,L}$, $B^{C,L}$, $A^{I,L}$, $A^{\Gamma,L}$, $A^{L,L}$, $B^{L,L}$ are not sparse, as the loop fields $\mathbf{T}_{0,n}$ can have a relatively large support.

The right hand side of the system is the (complex) vector

$$\begin{bmatrix} F^C + \imath\omega^{-1}G^C \\ F^I \\ F^\Gamma \\ F^L + \imath\omega^{-1}G^L \end{bmatrix},$$

whose dimension is $m_C + n_I + n_\Gamma - 1 + g$ and whose components are

$$\begin{aligned}
F^C_k &= -\int_{\Omega_C} \boldsymbol{\mu}\mathbf{H}_{e,h}\cdot\mathbf{w}_{h,k} \quad , \quad k = 1,\dots,m_C \\
G^C_k &= \int_{\Omega_C} \boldsymbol{\sigma}^{-1}(\operatorname{curl}\mathbf{H}_{e,h} - \mathbf{J}_e)\cdot\operatorname{curl}\mathbf{w}_{h,k} \quad , \quad k = 1,\dots,m_C \\
F^I_l &= -\int_{\Omega_I} \boldsymbol{\mu}\mathbf{H}_{e,h}\cdot\operatorname{grad}\Phi_{h,n_C+l} \quad , \quad l = 1,\dots,n_I \\
F^\Gamma_s &= -\int_{\Omega} \boldsymbol{\mu}\mathbf{H}_{e,h}\cdot\operatorname{grad}\Phi_{h,n_C+n_I+s} \quad , \quad s = 1,\dots,n_\Gamma - 1 \\
F^L_m &= -\int_{\Omega} \boldsymbol{\mu}\mathbf{H}_{e,h}\cdot\mathbf{T}_{0,m} \quad , \quad 1 \le m \le g\,, \\
G^L_m &= \int_{\Omega_C} \boldsymbol{\sigma}^{-1}(\operatorname{curl}\mathbf{H}_{e,h} - \mathbf{J}_e)\cdot\operatorname{curl}\mathbf{T}_{0,m} \quad , \quad 1 \le m \le g\,.
\end{aligned}$$

3.2. The algebraic solver

In a compact form, the linear system we have to solve has the following coefficient matrix

$$A - \imath\,\omega^{-1}B\,,$$

where A is real, symmetric and positive definite, while B is real, symmetric and positive semidefinite. Therefore $A - \imath\,\omega^{-1}B$ is a non-hermitian matrix, but it is complex symmetric. Clearly, passing to the complex conjugate, it is equivalent to consider a linear system associated to the matrix $A + \imath\,\omega^{-1}B$.

For the sake of definiteness, we will assume from now on that the frequency ω is strictly positive, and we focus on the linear system

$$(A + \imath\,\omega^{-1}B)\mathbf{z} = \mathbf{b}\,,$$

with $\mathbf{b}$ a complex vector. Efficient solvers for complex systems of this type have been devised in several papers, starting from Bai et al. [8]. The most suitable one is called Modified Hermitian and Skew-Hermitian Splitting (MHSS) method (see Bai et al. [9]), and can be formulated as follows: given an arbitrary initial guess $\mathbf{z}^0$, iterate according to the procedure

$$\begin{cases} (\alpha V + A)\mathbf{z}^{k+1/2} = (\alpha V - \imath\,\omega^{-1}B)\mathbf{z}^k + \mathbf{b} \\ (\alpha V + \omega^{-1}B)\mathbf{z}^{k+1} = (\alpha V + \imath\,A)\mathbf{z}^{k+1/2} - \imath\,\mathbf{b}\,, \end{cases}$$

having chosen a suitable real, symmetric and positive definite matrix V and a parameter $\alpha > 0$.

A possible, simple choice is $V = A$ and $\alpha = 1$ (see Bai et al. [10]), that can be shown to lead to the problem

$$(1+\imath)(A + \omega^{-1}B)(\mathbf{z}^{k+1} - \mathbf{z}^k) = \mathbf{b} - (A + \imath\,\omega^{-1}B)\mathbf{z}^k\,,$$

namely, a classical Richardson iteration with the preconditioner

$$P = (1+\imath)(A + \omega^{-1}B)\,.$$

Since the spectral properties of this preconditioner have been shown to be very good, it can be used inside a more efficient iterative method, like the COCG reported here below (see van der Vorst and Melissen [11]; see also van Rienen [12]).

In our computation we used this approach, with $P = A + \omega^{-1}B$, finding very effective convergence properties. Clearly, at each step of the iterative procedure we are left with the solution of a linear system associated to the matrix $A + \omega^{-1}B$, that, though symmetric and positive definite, is still bad conditioned.

In this respect, we have followed this strategy: if the number of unknowns is not too high, a Cholesky or, better, an incomplete Cholesky decomposition of $A+\omega^{-1}B$ is adopted; when the dimension of the matrix $A+\omega^{-1}B$ is large, some preconditioned conjugate gradient iterations are employed (but without needing to reach convergence; in our implementation, only one step is often used). Since $A+\omega^{-1}B$ is symmetric and positive definite, one has many options for the choice of the preconditioner. We have found very effective the use of suitable polynomial preconditioners as those proposed and analyzed in Bertolazzi and Frego [13].

Algorithm 1: COCG

$\boldsymbol{r} \leftarrow \boldsymbol{b} - \boldsymbol{A}\boldsymbol{x}$;
$\widetilde{\boldsymbol{r}} \leftarrow \boldsymbol{P}^{-1}\boldsymbol{r}$;
$\boldsymbol{p} \leftarrow \widetilde{\boldsymbol{r}}$;
$\rho \leftarrow [\widetilde{\boldsymbol{r}}, \boldsymbol{r}]$;
while $||\boldsymbol{r}|| > \varepsilon\,||\boldsymbol{b}||$ **do**
  $\boldsymbol{q} \leftarrow \boldsymbol{A}\boldsymbol{p}$;
  $\mu \leftarrow [\boldsymbol{q}, \boldsymbol{p}]$;
  $\alpha \leftarrow \rho/\mu$;
  $\boldsymbol{x} \leftarrow \boldsymbol{x} + \alpha\,\boldsymbol{p}$;
  $\boldsymbol{r} \leftarrow \boldsymbol{r} - \alpha\,\boldsymbol{q}$;
  $\widetilde{\boldsymbol{r}} \leftarrow \boldsymbol{P}^{-1}\boldsymbol{r}$;
  $\beta \leftarrow \rho$;
  $\rho \leftarrow [\widetilde{\boldsymbol{r}}, \boldsymbol{r}]$;
  $\beta \leftarrow \rho/\beta$;
  $\boldsymbol{p} \leftarrow \widetilde{\boldsymbol{r}} + \beta\,\boldsymbol{p}$;
end while

4. Numerical experiments

In the following we present some numerical experiments in order to evaluate the performance of the proposed method. First we consider a problem with a known analytical solution to validate the code and to test the convergence properties of the method. The second experiment is benchmark problem number 7 in the TEAM workshop, which deals with an asymmetrical conductor with a hole (see Fujiwara and Nakata [14], Kanayama et al. [15]). In the last set of numerical experiments the geometry of the conductor corresponds to a three-phase power transformer: a classical five-leg one or the Hexaformer transformer (see Tidblad Lundmark [16]). This last transformer has a special shape of the core: it consists of nine rolls of laminated steel bands and the core legs have a cross section of hexagonal shape.

4.1. A problem with a known analytical solution

Given the computational domain $\Omega = (-a,a)\times(-b,b)\times(-c,c) \subset \mathbb{R}^3$, a vector field of the form $\mathbf{E}^*(\mathbf{x}) = f(\mathbf{x})\mathbf{G}(\mathbf{x})$, with $f(\mathbf{x})$ a scalar (smooth) function and $\mathbf{G}(\mathbf{x}) = \begin{bmatrix} 0 \\ 0 \\ (x_1^2-a^2)(x_2^2-b^2) \end{bmatrix}$, clearly satisfy $\mathbf{E}^*\times\mathbf{n} = \mathbf{0}$ on $\partial\Omega$. Let us set

$$\mathbf{H}^*(\mathbf{x}) = i(\omega\mu)^{-1}\operatorname{curl}\mathbf{E}^*(\mathbf{x}) = i(\omega\mu)^{-1}\left(\operatorname{grad} f(\mathbf{x})\times\mathbf{G}(\mathbf{x}) + f(\mathbf{x})\operatorname{curl}\mathbf{G}(\mathbf{x})\right)$$

$$= i(\omega\mu)^{-1}\begin{bmatrix} \left((x_2^2-b^2)\frac{\partial f}{\partial x_2}(\mathbf{x}) + 2\,x_2\,f(\mathbf{x})\right)(x_1^2-a^2) \\ -\left((x_1^2-a^2)\frac{\partial f}{\partial x_1}(\mathbf{x}) + 2\,x_1\,f(\mathbf{x})\right)(x_2^2-b^2) \\ 0 \end{bmatrix}.$$

If, for instance, the magnetic permeability μ is smooth, we can set $\mathbf{J}_e = \operatorname{curl}\mathbf{H}^* - \sigma\mathbf{E}^*$. Then the couple $(\mathbf{E}^*, \mathbf{H}^*)$ is solution of the eddy current problem (4).

In this specific test problem we set $a = 4$, $b = 3$ and $c = 3$, the scalar function

$$f(\mathbf{x}) = 10^{-4} \sin\left(2\pi\left(\frac{x_1}{a} + \frac{x_2}{b} + \frac{x_3}{c}\right)\right),$$

and the parameters $\omega = 2\pi \times 50$, $\mu = 4\pi \times 10^{-7}$, $\sigma = 4 \times 10^7$.

We consider two different situations: in the first case the conducting region has two connected components (a torus and a granny knot), and they are linked; in the second one the conducting region is just the torus. Both problems have the same exact solution $(\mathbf{E}^*, \mathbf{H}^*)$: so they have different sources $\mathbf{J}_e = \operatorname{curl} \mathbf{H}^* - \sigma \mathbf{E}^*$, being different the region where σ is different from 0, and thus the overall solution algorithm is based on different steps. These geometrical configurations present two independent loop fields in the first case, and one independent loop field in the second case.

In Figure 1 we show the two linked conductors (left) and the toroidal conductor (right).

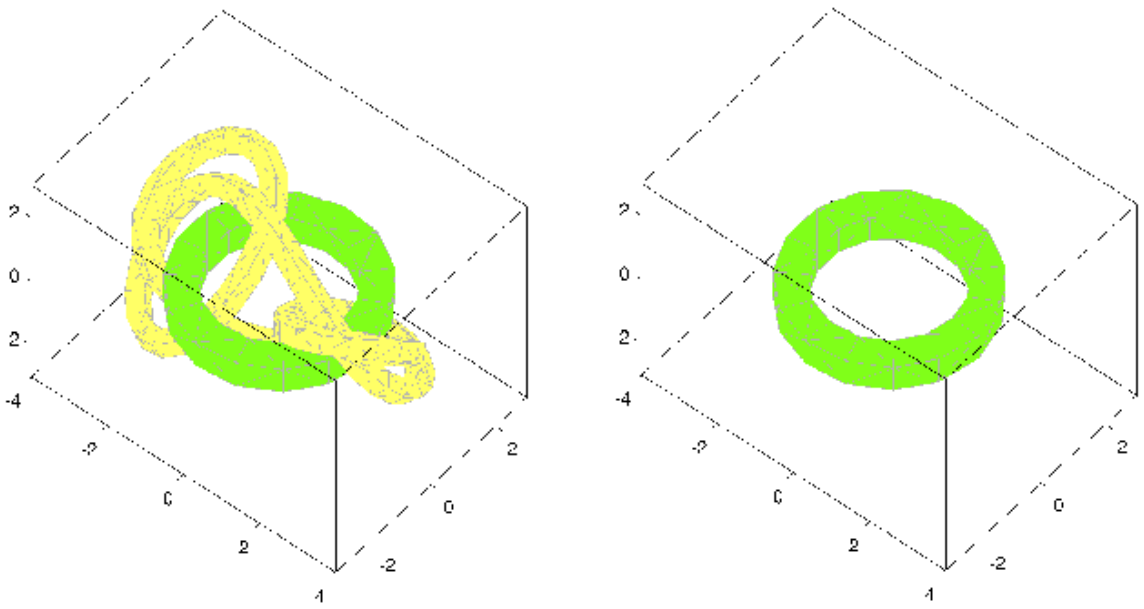

Figure 1: Two geometrical settings for the problem with a known analytical solution.

The code has been tested by solving these problems with successive uniformly refined meshes. We performed the test with the two linked conductors using four different meshes, then we repeated the test with the same meshes but fixing the conductivity equal to 0 in the granny knot. Finally, we also solved the problem with the toroidal conductor only, but remeshing the insulator. In this case we used five different meshes. Figure 2 shows the plot in the log-log scale of the relative error $e^c_{\mathbf{H}} = \frac{\|\mathbf{H}-\mathbf{H}_h\|_{H(\mathrm{curl};\Omega)}}{\|\mathbf{H}\|_{H(\mathrm{curl};\Omega)}}$ versus the normalized mesh size h/h_0, being h_0 the mesh size of the coarsest mesh. Linear convergence can be observed in all cases.

In Table 1, Table 2 and Table 3 we report the number of elements, the number of degrees of freedom, the relative error in $(L^2(\Omega))^3$-norm ($e^{L2}_{\mathbf{H}} = \frac{\|\mathbf{H}-\mathbf{H}_h\|_{0,\Omega}}{\|\mathbf{H}\|_{0,\Omega}}$), the relative error $e^c_{\mathbf{H}}$ in $H(\mathrm{curl};\Omega)$-norm, and the computational time for the three considered situations. Notice that the accuracy of the numerical solution and the computational time do not depend on the topology of the conductor.

In Figure 3 we compare pointwise values of the exact solution and of the reconstructed numerical solution in the three cases previously considered.

Since edge elements are not well-suited for pointwise evaluation (their degrees of freedom are line integrals, and their normal components can jump on the interface between different elements), here and in the sequel we have indeed "reconstructed" the obtained numerical solution.

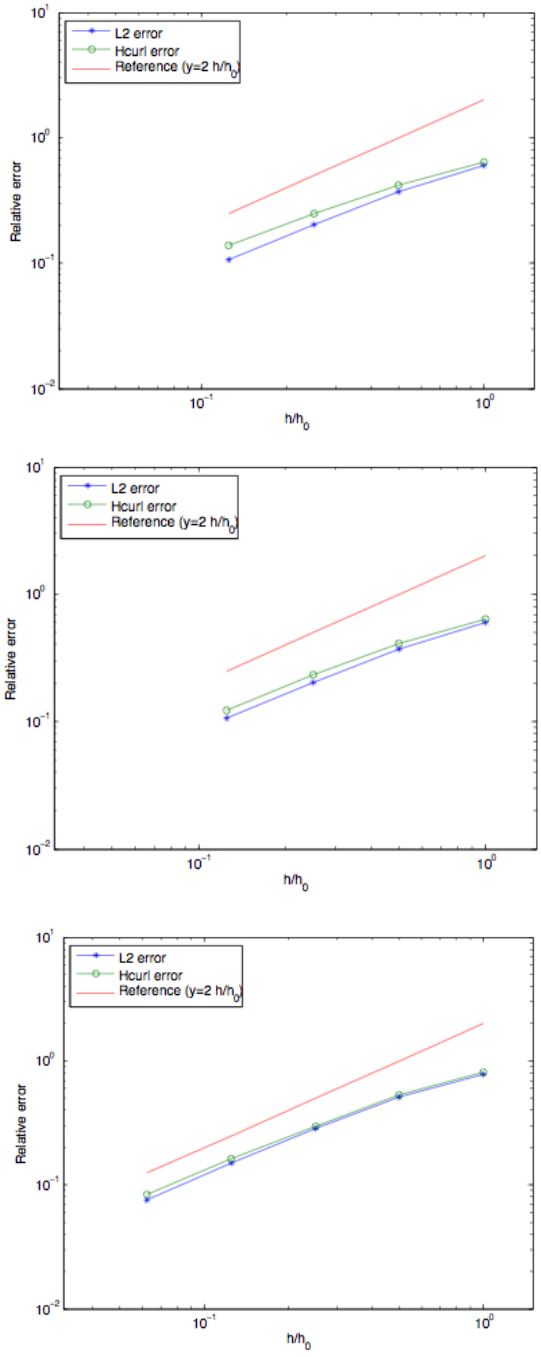

Figure 2: Relative error versus normalized mesh size h/h_0. From the top: linked conductors, toroidal conductor using the same meshes of the case of linked conductors, and toroidal conductor with new meshes in the insulator.

The reconstruction $\widehat{\mathbf{v}}_h$ of a Nédélec vector function $\mathbf{v}_h$ is computed in the following way. For each vertex $\mathbf{p}$ of the mesh, we denote by $T(\mathbf{p})$ the set of tetrahedra having $\mathbf{p}$ as a vertex, and we define $\widehat{\mathbf{v}}_h$ as the

Elem.	DoF	$e_{\mathbf{H}}^{L2}$	$e_{\mathbf{H}}^{c}$	CPU time [s]
6386	1867	0.605604	0.637105	124×10^{-3}
51088	16865	0.371734	0.417951	142×10^{-2}
408704	143295	0.202935	0.246137	214×10^{-1}
3269632	1181115	0.105956	0.139175	319×10^{0}

Table 1: Results for the problem with a known analytical solution. Linked conductors.

Elem.	DoF	$e_{\mathbf{H}}^{L2}$	$e_{\mathbf{H}}^{c}$	CPU time [s]
6386	1812	0.606396	0.634212	134×10^{-3}
51088	16132	0.372723	0.409549	144×10^{-2}
408704	136238	0.203468	0.232320	170×10^{-1}
3269632	1119866	0.106155	0.123747	311×10^{0}

Table 2: Results for the problem with a known analytical solution. Toroidal conductor - same meshes.

Elem.	DoF	$e_{\mathbf{H}}^{L2}$	$e_{\mathbf{H}}^{c}$	CPU time [s]
1213	298	0.787179	0.810539	150×10^{-4}
9704	2345	0.512298	0.531710	163×10^{-3}
77632	18824	0.283124	0.299748	143×10^{-2}
621056	151246	0.148604	0.161413	187×10^{-1}
4968448	1213338	0.075791	0.083637	309×10^{0}

Table 3: Results for the problem with a known analytical solution. Toroidal conductor with new meshes in the insulator.

piecewise-linear interpolant of the values

$$\widehat{\mathbf{v}}_h(\mathbf{p}) = \frac{\displaystyle\sum_{t \subset T(\mathbf{p})} \int_t \mathbf{v}_h}{\displaystyle\sum_{t \subset T(\mathbf{p})} \mathrm{meas}(t)} \,.$$

An alternative way of reconstruction is also possible. We denote by $E(\mathbf{p})$ the set of edges having $\mathbf{p}$ as a vertex, and by $d_e(\mathbf{v}_h)$ the degree of freedom of $\mathbf{w}_h$ associated to the edge e, namely, $\int_e \mathbf{v}_h \cdot \boldsymbol{\tau}_e$ with $\boldsymbol{\tau}_e$ the unit tangent vector on e. The reconstruction $\widetilde{\mathbf{v}}_h$ is defined as the piecewise-linear interpolant of the values $\widetilde{\mathbf{v}}_h(\mathbf{p})$ obtained by solving in the least squares sense the linear system

$$\widetilde{\mathbf{v}}_h(\mathbf{p}) \cdot \boldsymbol{\tau}_e \,\mathrm{meas}(e) = d_e(\mathbf{v}_h) \quad \forall\, e \subset E(\mathbf{p}) \,.$$

We have used both methods without noting significant differences in the plotted results.

For the finest mesh we show in Figure 3 the imaginary part of the first component of the magnetic field along the x-axis. It can be clearly observed that the accuracy of the proposed method does not depend on the topology of the conductor, and that the exact solution is perfectly recovered in all the geometrical configurations.

4.2. Benchmark problem 7 in the TEAM workshop

The second test problem is the classical benchmark problem number 7 in the TEAM workshop (see Fujiwara and Nakata [14]; for more recent numerical results about this problem, with different formulations, see, e.g., Alonso Rodríguez and Vázquez Hernández [17], Ledger and Zaglmayr [18]). It consists of a thick

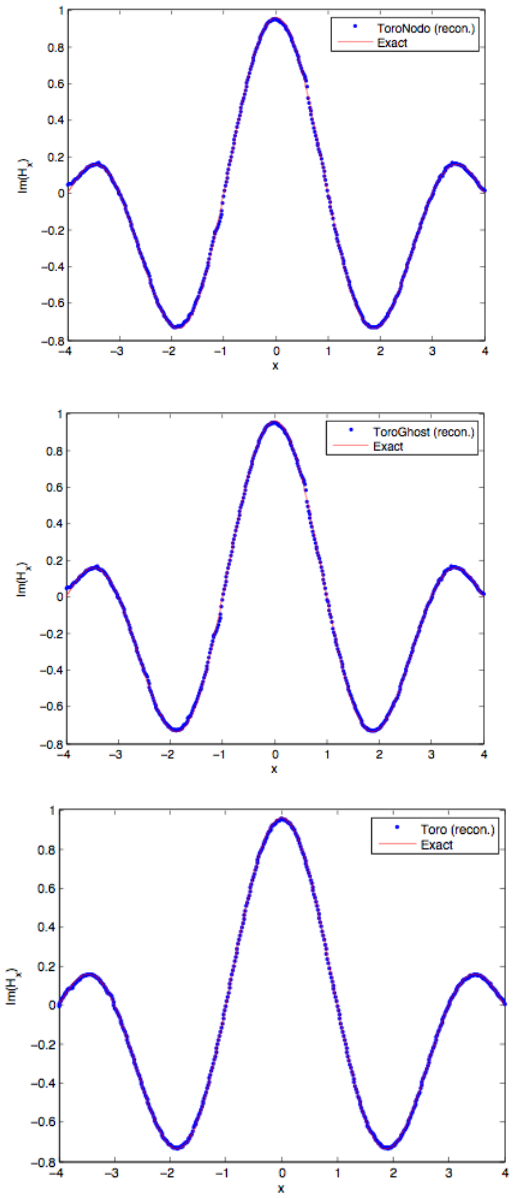

Figure 3: x-component of Im($\mathbf{H}$) along the x-axis: the exact solution and the numerical solutions in the finest mesh. From the top: linked conductors, toroidal conductor using the same meshes of the case of linked conductors, and toroidal conductor with new meshes in the insulator.

aluminum plate with an eccentrically placed hole, subjected to an asymmetric magnetic field. The field is produced by an exciting current supported in a coil above the plate. For the geometrical description see Figure 4 (length is expressed in millimeters); we have only one independent loop field. The plate and the coil are strictly inside the computational domain, which is the hexahedron $(-200, 600)\times(-200, 600)\times(-200, 400)$.

The angular frequency is $\omega = 2\pi \times 50$ rad/s, the magnetic permeability is $\mu = \mu_0 = 4\pi \times 10^{-7}$ H/m, the electrical conductivity is $\sigma = 3.526 \times 10^7$ S/m, and the absolute value of the real part (respectively, imaginary part) of the excitation current density $\mathbf{J}_e$ is 1.0968×10^6 (respectively 0) A/m^2. The positive direction of the current in the coil is counter-clockwise as seen from the top.

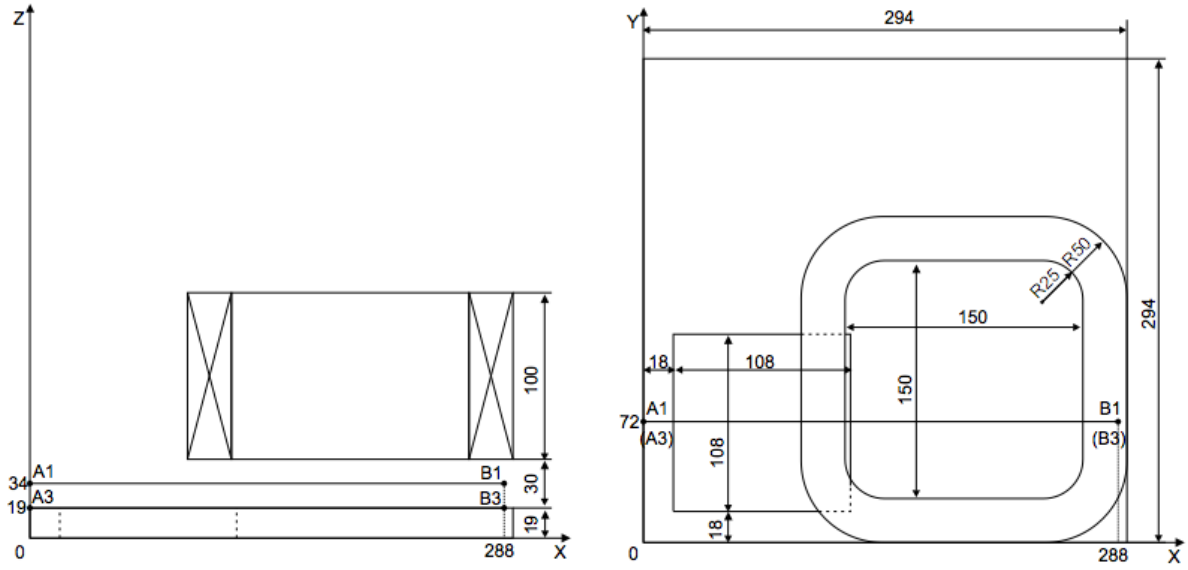

Figure 4: Geometry of benchmark problem in the TEAM workshop.

In Figure 5 we plot the experimental data given in Fujiwara and Nakata [14] and the reconstruction of the solution for three different meshes. On the left we report the z-component of the magnetic induction $\mathbf{B}$, more precisely $\text{sign}(\text{Re}(\mathbf{B}_z))|\mathbf{B}_z|$, along a straight line contained in the air region, with $y = 72$ mm and $z = 34$ mm (line A1-B1); on the right we present the y-component of the current density $\mathbf{J} = \text{curl}\,\mathbf{H}$, more precisely $\text{sign}(\text{Re}(\mathbf{J}_y))|\mathbf{J}_y|$, along a straight line on the surface of the conductor, with $y = 72$ mm and $z = 19$ mm (line A3-B3).

Note that here we are showing the reconstruction of the numerical approximation of $\mathbf{J} = \text{curl}\,\mathbf{H}$, namely, of a Raviart–Thomas face element. For a function $\mathbf{w}_h \in RT_h$ this reconstruction is done in the following way. We denote by $F(\mathbf{p})$ the set of faces having $\mathbf{p}$ as a vertex, and by $d_f(\mathbf{w}_h)$ the degree of freedom of $\mathbf{w}_h$ associated to the face f, namely, $\int_f \mathbf{w}_h \cdot \mathbf{n}_f$ with $\mathbf{n}_f$ the unit normal vector on f. We define $\widetilde{\mathbf{w}}_h$ as the piecewise-linear interpolant of the values $\widetilde{\mathbf{w}}_h(\mathbf{p})$ obtained by solving in the least squares sense the linear system

$$\widetilde{\mathbf{w}}_h(\mathbf{p}) \cdot \mathbf{n}_f \,\text{meas}(f) = d_f(\mathbf{w}_h) \quad \forall\ f \subset F(\mathbf{p})\,.$$

Table 4 shows the computational cost for the three considered meshes. It gives the number of elements, edges and vertices, and the number of degrees of freedom for each mesh. We have also reported the number of degrees of freedom of the most used formulation for eddy current problems, namely, the magnetic vector potential/electric scalar potential formulation $(\mathbf{A}_C, V_C)$-$\mathbf{A}_I$ (without gauging). We recall that the number of degrees of freedom of our approach is the number of edges in the conductor plus the number of vertices in the insulator plus g (the first Betti number of Ω_I). Instead, in the ungauged $(\mathbf{A}_C, V_C)$-$\mathbf{A}_I$ formulation the number of degrees of freedom is the total number of edges plus the number of vertices in the conductor. It is thus apparent that the number of unknowns in our approach is much less than in this classical approach.

The table shows also the computational time for the preprocessing part of the algorithm (construction of non-bounding cycles, loop fields and source field) and the computational time for solving the linear system. It is worth noting that the computational time for the solution of the linear system associated to our formulation is quite satisfactory, while one has to remember that the ungauged $(\mathbf{A}_C, V_C)$-$\mathbf{A}_I$ formulation must face the solution of a singular linear system, and this needs some computational care. Notice also that the preprocessing time is small compared with the time required for solving the linear system.

To conclude this example, in Figure 6 we show the three components of the eddy current on the surface

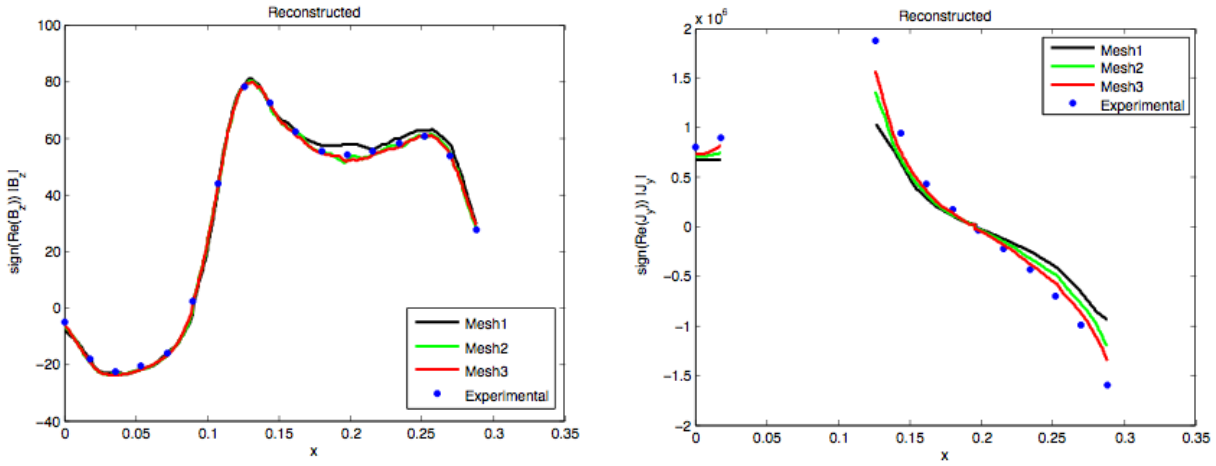

Figure 5: z-component of $\mathbf{B}$ along line A1-B1 (left) and y-component of $\mathbf{J}$ along line A3-B3 (right), for three successively refined meshes.

	Mesh 1	Mesh 2	Mesh 3
Elements	156418	1251344	10010752
Edges	184430	1466234	11701668
Vertices	27197	211627	1677861
DoF	28268	222900	1778886
DoF $(\mathbf{A}_C, V_C)$-$\mathbf{A}_I$	185113	1470026	11725948
Preprocessing CPU time [s]	1.907	17.83	149.9
Linear algebra CPU time [s]	4.921	67.82	714.4

Table 4: Mesh data and computational cost for solving problem 7 in the TEAM workshop.

of the conducting plate, namely, $\text{sign}(\text{Re}(\mathbf{J}_x))|\mathbf{J}_x|$, $\text{sign}(\text{Re}(\mathbf{J}_y))|\mathbf{J}_y|$ and $\text{sign}(\text{Re}(\mathbf{J}_z))|\mathbf{J}_z|$ (note that in the third figure we use a different scale, as the third component of the eddy current is much smaller than the other two).

4.3. Three-phase power transformer

In this section we consider a three-phase transformer. Since our aim is mainly focused on emphasizing the topological aspects of the problem, we deal indeed with a simplified linear isotropic problem, a situation that does not describe real devices (for numerical simulations in a more general situation, see, e.g., Preis et al. [19], Bíró et al. [20]). We consider two different geometrical models: a classical five-leg transformer and the Hexaformer transformer (see Tidblad Lundmark [16]). In the first model there are 4 independent loop fields, while in the second one the number of independent loop fields is 16.

4.3.1. Five-leg transformer

The computational domain is the hexahedron $(-400, 400) \times (-200, 200) \times (-300, 300)$ (lengths are expressed in millimeters). Also in this case we consider the angular frequency $\omega = 2\pi \times 50$ rad/s. The conductivity in the core is $\sigma = 10^7$ S/m. The applied current density is 10^6 A/m^2 in the first coil, $10^6(\cos\frac{2\pi}{3} + i\sin\frac{2\pi}{3})$ A/m^2 in the second one, and $10^6(\cos\frac{4\pi}{3} + i\sin\frac{4\pi}{3})$ A/m^2 in the third one. The magnetic permeability in the non-conducting region is $\mu = \mu_0 = 4\pi \times 10^{-7}$ H/m, while in the core it is $\mu = \mu_r\mu_0$, being μ_r the relative permeability. The geometry is described in Figure 7.

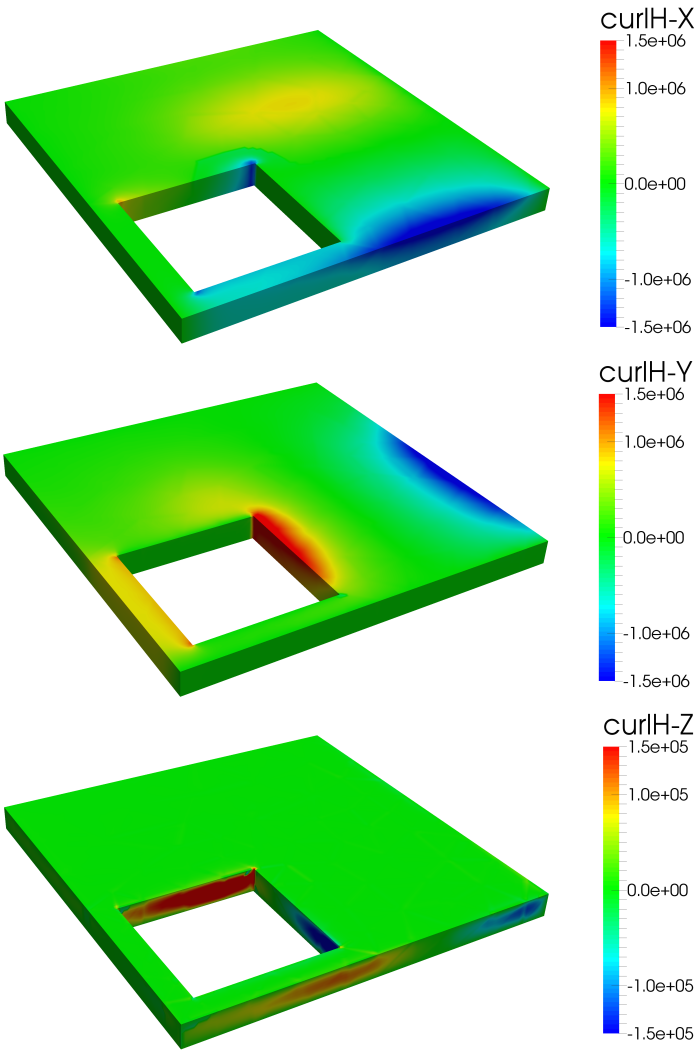

Figure 6: The three components of the eddy current on the surface of the conducting plate.

In order to display the skin effect, we consider three different situations: $\mu_r = 2$, $\mu_r = 20$, and $\mu_r = 200$. A good approximation for the skin depth is given by $\delta = \sqrt{\frac{2}{\omega\sigma\mu}}$, hence $\delta = \frac{1}{2\pi}\frac{1}{\sqrt{50\mu_r}}$ m, namely, $\delta \approx 1.6$ cm if $\mu_r = 2$, $\delta \approx 0.5$ cm if $\mu_r = 20$ and $\delta \approx 1.6$ mm if $\mu_r = 200$. Close to the boundary of the core, the used mesh must be fine enough to capture this effect: for this reason, we use a finer mesh in the case $\mu_r = 200$. Figure 8 shows the average eddy current along a period, namely,

$$\left(\frac{\omega}{2\pi}\int_0^{2\pi/\omega} |\sigma(\mathbf{x})\mathcal{E}(\mathbf{x},t)|^2\,dt\right)^{1/2} = \left(\frac{1}{2}\left(|\mathrm{Re}(\sigma(\mathbf{x})\mathbf{E}(\mathbf{x}))|^2 + |\mathrm{Im}(\sigma(\mathbf{x})\mathbf{E}(\mathbf{x}))|^2\right)\right)^{1/2},$$

for the five-leg transformer with $\mu_r = 2$, $\mu_r = 20$, and $\mu_r = 200$, respectively.

Figure 9 shows the magnetic field at three different times ($\omega t = 0$, $\omega t = 2\pi/3$ and $\omega t = 4\pi/3$) for the five-leg transformer with $\mu_r = 200$.

Table 5 reports the number of elements, edges and vertices, and the number of degrees of freedom for the two different meshes. As before, for comparison we also report the number of degrees of freedom of the

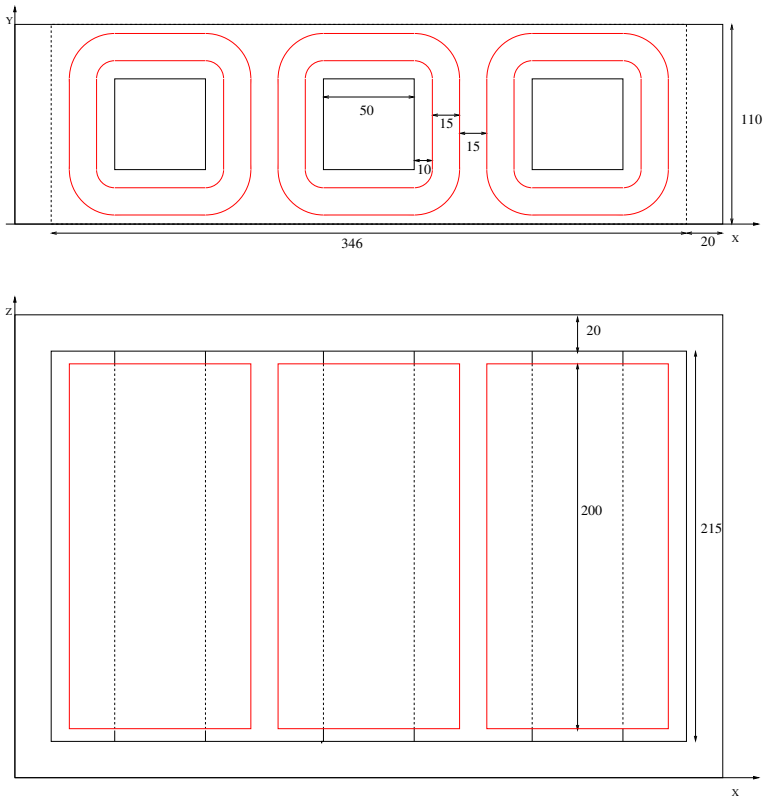

Figure 7: The geometry of the five-leg transformer (the coils are in red).

$(\mathbf{A}_C, V_C)$-$\mathbf{A}_I$ approach.

	$\mu = 2$ and $\mu = 20$	$\mu = 200$
Elements	589858	1496208
Edges	694993	1746424
Vertices	99579	244706
DoF	402717	1299199
DoF $(\mathbf{A}_C, V_C)$-$\mathbf{A}_I$	767291	1961147

Table 5: Mesh data for the five-leg transformer.

Table 6 shows the computational time for the preprocessing part of the algorithm (including, as in the case of problem 7 in the TEAM workshop, the construction of non-bounding cycles, loop fields and source field) and the computational time for solving the linear system for the three values of μ_r. Again, the preprocessing time is small compared with the solution of the linear system and with the overall computational cost.

	$\mu_r = 2$	$\mu_r = 20$	$\mu_r = 200$
Preprocessing CPU time [s]	≈ 10	≈ 10	≈ 18
Linear algebra CPU time [s]	≈ 310	≈ 247	≈ 1200

Table 6: Computational cost for the five-leg transformer, for three different values of μ_r.

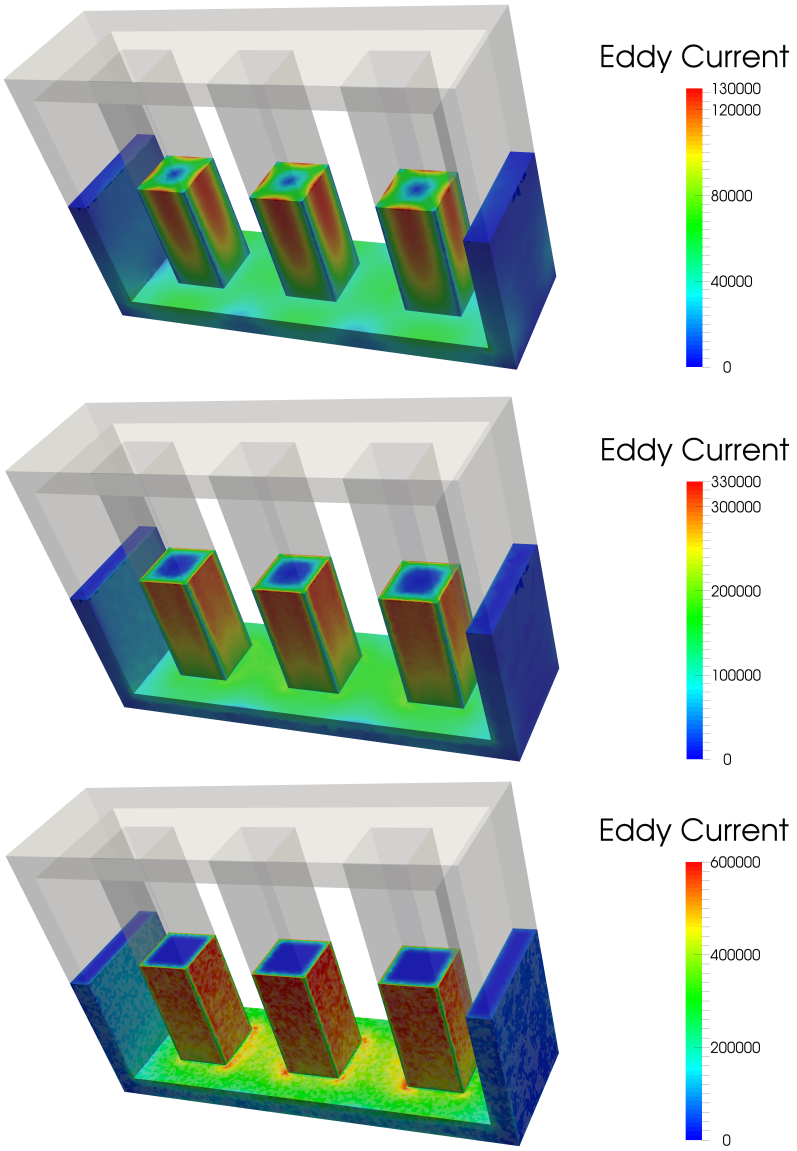

Figure 8: The average eddy current along a period for the five-leg transformer with $\mu_r = 2$, $\mu_r = 20$ and $\mu_r = 200$, respectively.

4.3.2. Hexaformer transformer

The computational domain is the hexahedron $(-200, 200) \times (-200, 200) \times (-400, 400)$ (lengths are expressed in millimeters). The height of the legs and of the coils is 205 mm. For the other dimensions see Figure 10, representing a horizontal section; for a more detailed description of the geometry, especially in the part of the core connecting the three legs, we refer to Tidblad Lundmark [16].

We show in Figure 11, top left, the geometry of the core and the automatically generated 16 non-bounding cycles in the non-conducting region, namely, the cycles that are necessary for the construction of the loop fields.

As in the previous examples the angular frequency is $\omega = 2\pi \times 50$ rad/s, the conductivity in the core is $\sigma = 10^7$ S/m and the applied current density is 10^6 A/m^2 in the first coil, $10^6(\cos\frac{2\pi}{3} + i\sin\frac{2\pi}{3})$ A/m^2 in the second one, and $10^6(\cos\frac{4\pi}{3} + i\sin\frac{4\pi}{3})$ A/m^2 in the third one. The magnetic permeability in the

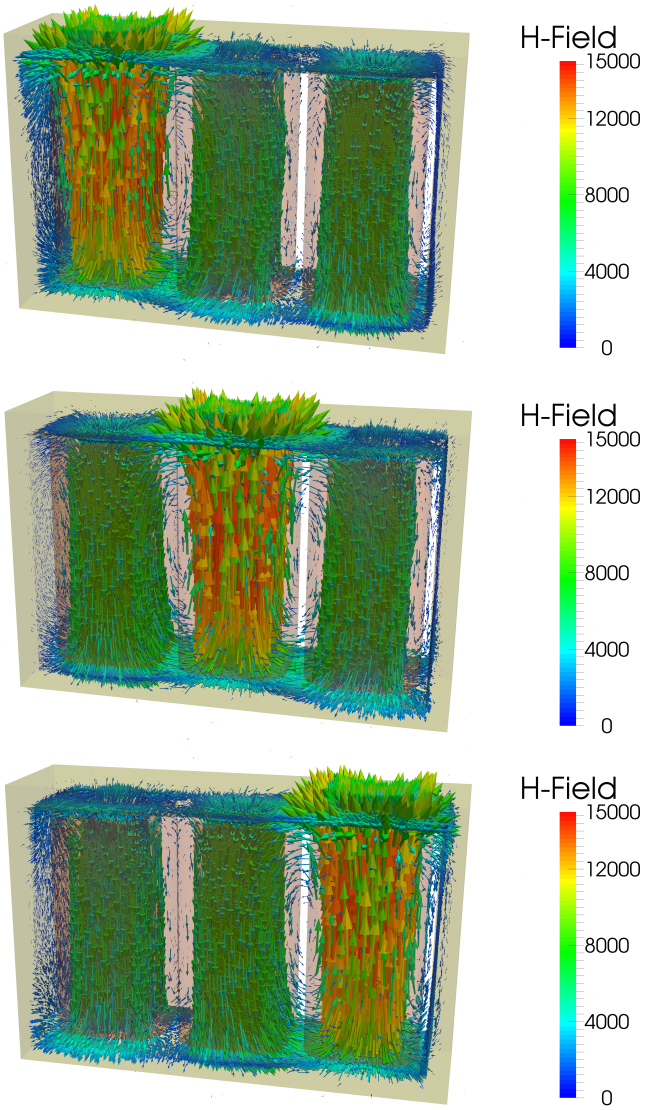

Figure 9: The magnetic field at $\omega t = 0$, $\omega t = 2\pi/3$ and $\omega t = 4\pi/3$ for the five-leg transformer with $\mu_r = 2$.

non-conducting region is $\mu = \mu_0 = 4\pi \times 10^{-7}$ H/m, while in the core it is $\mu = \mu_r \mu_0$, with $\mu_r = 2$ or $\mu_r = 20$.

Figure 11, middle and bottom left, shows the average eddy current along a period for $\mu_r = 2$ (middle) and $\mu_r = 20$ (bottom). The variation of the skin depth can be clearly observed.

In Figure 11, right, we show the magnetic field at three different times ($\omega t = 0$, $\omega t = 2\pi/3$ and $\omega t = 4\pi/3$) with $\mu_r = 2$. Also in this case we report in Table 7 the number of elements, edges and vertices, and the number of degrees of freedom and, for comparison, the number of degrees of freedom of the $(\mathbf{A}_C, V_C)$-$\mathbf{A}_I$ approach. Table 8 shows the computational cost for $\mu_r = 2$ and $\mu_r = 20$.

5. Conclusion

In this paper we have presented a finite element method for the approximation of the solution of the eddy current problem. The magnetic field in the non-conducting region is expressed as the sum of a gradient

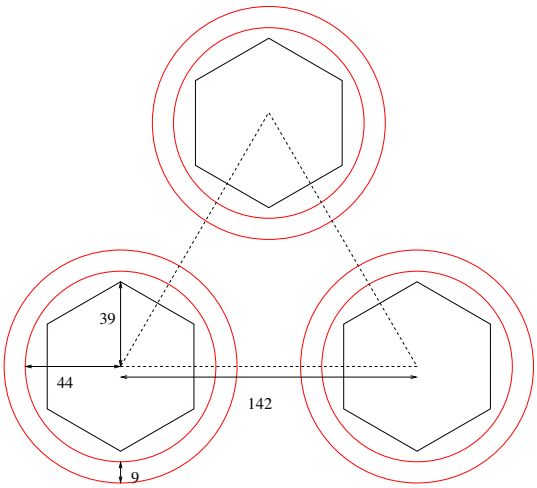

Figure 10: The geometry of the Hexaformer transformer (a horizontal section is drawn; the coils are in red).

Elements	4092408
Edges	4924236
Vertices	804637
DoF	2065494
DoF $(\mathbf{A}_C, V_C)$-$\mathbf{A}_I$	5232667

Table 7: Mesh data for the Hexaformer transformer.

	$\mu_r = 2$	$\mu_r = 20$
Preprocessing CPU time [s]	≈ 200	≈ 200
Linear algebra CPU time [s]	≈ 8500	≈ 6300

Table 8: Computational cost for the Hexaformer transformer, for two different values of μ_r.

and a term which is present only when the topological shape of the non-conducting domain is not trivial. In this way the number of degrees of freedom is much lower than in a classical approximation method using edge elements in the whole computational domain.

The construction of a finite element basis is shown to be an easy task, as the basis functions taking into account the topological shape can be constructed in a simple way just knowing the structure of the mesh in the non-conducting domain. The construction of the so-called "cutting" surfaces is not needed, thus simplifying in a significant way the overall procedure.

The resulting linear system can be solved by standard iterative methods for a complex symmetric matrix. The number of iterations needed for reaching convergence turns out to be relatively small, as for a complex symmetric matrix it is known how to find good preconditioners.

The numerical results show a really satisfactory performance of the proposed method; one of the most interesting features is that the topological shape of the non-conducting domain does not give rise to significative problems, as it is quite cheap to perform the preprocessing computational part, in which we first construct the complete set of finite element basis functions, including those of topological type, and then the matrix related the linear system to be solved.

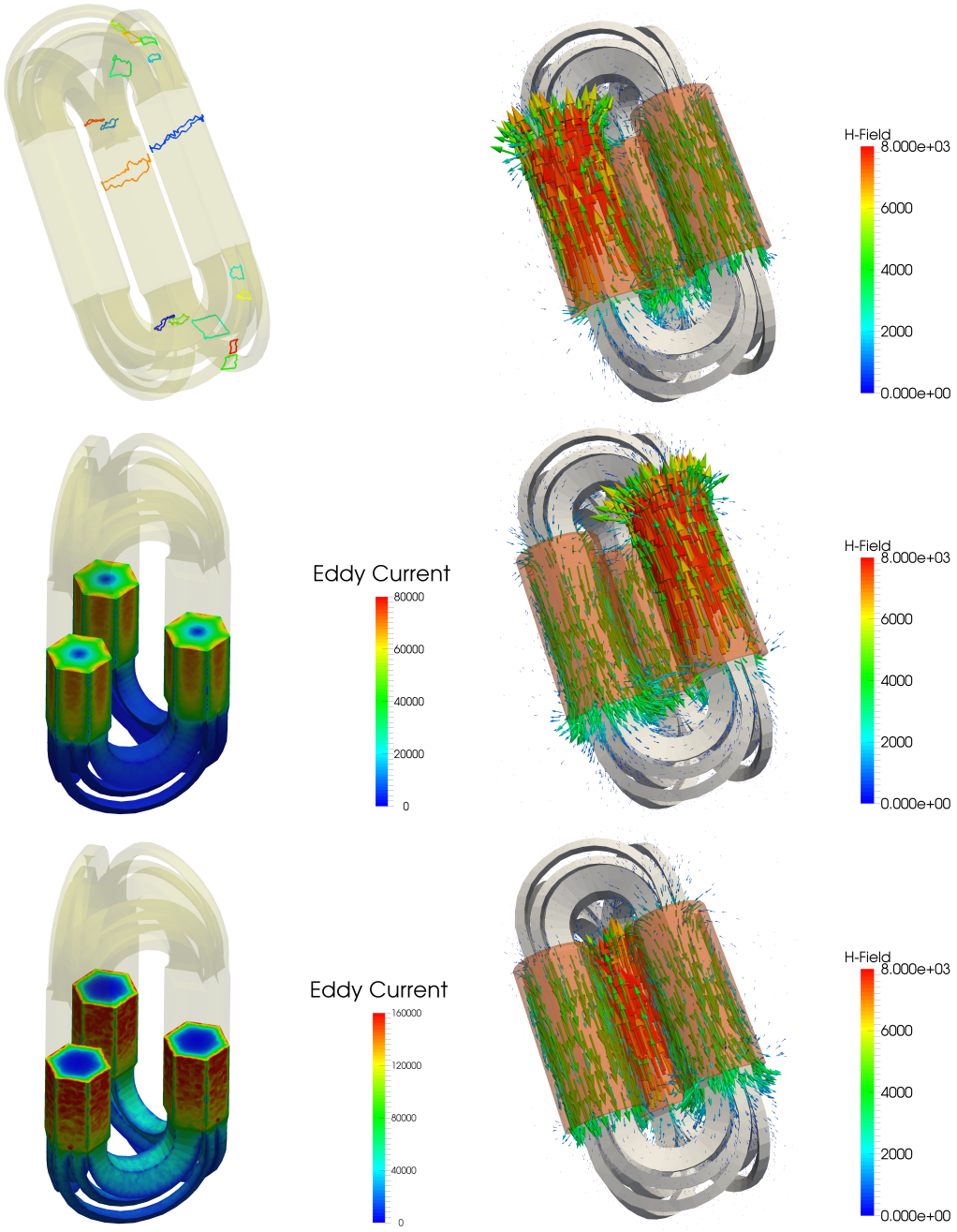

Figure 11: On the left from the top the non-bounding cycles in the insulator for the Hexaformer transformer, and the average eddy current along a period with $\mu_r = 2$ and $\mu_r = 20$. On the right from the top the magnetic field at $\omega t = 0$, $\omega t = 2\pi/3$ and $\omega t = 4\pi/3$ for the Hexaformer transformer with $\mu_r = 2$.

References

[1] A. Alonso Rodríguez, A. Valli, Eddy Current Approximation of Maxwell Equations, Springer-Verlag Italia, Milan, 2010.

[2] M. Costabel, M. Dauge, S. Nicaise, Corner singularities of Maxwell interface and eddy current problems, in: I. Gohberg, A. F. dos Santos, F.-O. Speck, F. S. Teixeira, W. Wendland (Eds.), Operator Theoretical Methods and Applications to Mathematical Physics, Birkhäuser Verlag, Basel, 2004, pp. 241–256.

[3] A. Bossavit, Computational Electromagnetism, Academic Press, San Diego, 1998.
[4] A. Bermúdez, R. Rodríguez, P. Salgado, A finite element method with Lagrange multipliers for low-frequency harmonic Maxwell equations, SIAM J. Numer. Anal. 40 (5) (2002) 1823–1849.
[5] A. Alonso Rodríguez, E. Bertolazzi, R. Ghiloni, A. Valli, Construction of a finite element basis of the first de Rham cohomology group and numerical solution of 3D magnetostatic problems, SIAM J. Numer. Anal. 51 (4) (2013) 2380–2402.
[6] R. Benedetti, R. Frigerio, R. Ghiloni, The topology of Helmholtz domains, Expo. Math. 30 (4) (2012) 319–375.
[7] P. Monk, Finite Element Methods for Maxwell's Equations, Oxford University Press, Oxford, 2003.
[8] Z.-Z. Bai, G. H. Golub, M. K. Ng, Hermitian and skew-Hermitian splitting methods for non-Hermitian positive definite linear systems, SIAM J. Matrix Anal. Appl. 24 (3) (2003) 603–626.
[9] Z.-Z. Bai, M. Benzi, F. Chen, Modified HSS iteration methods for a class of complex symmetric linear systems, Computing 87 (3-4) (2010) 93–111.
[10] Z.-Z. Bai, M. Benzi, F. Chen, On preconditioned MHSS iteration methods for complex symmetric linear systems, Numer. Algorithms 56 (2) (2011) 297–317.
[11] H. A. van der Vorst, J. B. M. Melissen, A Petrov-Galerkin type method for solving $Ax = b$, where A is symmetric complex, IEEE Trans. Magn. 26 (2) (1990) 706–708.
[12] U. van Rienen, Numerical Methods in Computational Electrodynamics, Springer-Verlag, Berlin, 2001.
[13] E. Bertolazzi, M. Frego, Preconditioning complex symmetric linear systems (2014). arXiv:1405.6297.
[14] K. Fujiwara, T. Nakata, Results for benchmark problem 7 (asymmetrical conductor with a hole), COMPEL 9 (1990) 137–154.
[15] H. Kanayama, D. Tagami, M. Saito, F. Kikuchi, A numerical method for 3-D eddy current problems, Japan J. Indust. Appl. Math. 18 (2) (2001) 603–612.
[16] S. Tidblad Lundmark, Computer model of electromagnetic phenomena in Hexaformer, Tech. rep., Department of Materials and Manufacturing Technology, Chalmers University of Technology (2007).
[17] A. Alonso Rodríguez, R. Vázquez Hernández, Iterative methods for the saddle-point problem arising from the $\mathbf{H}_C/\mathbf{E}_I$ formulation of the eddy current problem, SIAM J. Sci. Comput. 31 (4) (2009) 3155–3178.
[18] P. D. Ledger, S. Zaglmayr, *hp*-finite element simulation of three-dimensional eddy current problems on multiply connected domains, Comput. Methods Appl. Mech. Engrg. 199 (49-52) (2010) 3386–3401.
[19] K. Preis, O. Bíró, G. Buchgraber, I. Tičar, Thermal-electromagnetic coupling in the finite-element simulation of power transformers, IEEE Trans. Magn. 42 (4) (2006) 999–1002.
[20] O. Bíró, G. Koczka, K. Preis, Finite element solution of nonlinear eddy current problems with periodic excitation and its industrial applications, Appl. Numer. Math. 79 (2014) 3–17.